Integrated micro ring resonator displacement sensor for scanning probe microscopies

To cite this article: Isa Kiyat *et al* 2004 *J. Micromech. Microeng.* **14** 374

View the article online for updates and enhancements.

Related content

- Topical Review
  Andrew Yacoot and Ludger Koenders
- In-line Optical Lever System for Ultrasmall Cantilever Displacement Detection
  Atsushi Kikukawa, Hajime Koyanagi, Kimitoshi Etoh et al.
- Design and characterization of a micromachined Fabry--Perot vibration sensor for high-temperature applications
  P M Nieva, N E McGruer and G G Adams

Recent citations

- Optimization of Pulley-Type Ring Resonator with Waveguide Offset
  Meng-Hua Yen *et al*
- Integrated optical displacement sensor based on asymmetric Mach–Zehnder interferometer chip
  Ning Zhao *et al*
- Design and analysis of serially coupled double microring resonator based force sensor for 1N range measurement
  Venkateswara Rao Kolli *et al*

IOP ebooks™

Bringing you innovative digital publishing with leading voices to create your essential collection of books in STEM research.

Start exploring the collection - download the first chapter of every title for free.

This content was downloaded from IP address 139.179.72.51 on 29/12/2018 at 16:46

J. Micromech. Microeng. **14** (2004) 374–381 PII: S0960-1317(04)66502-8

Integrated micro ring resonator displacement sensor for scanning probe microscopies

Isa Kiyat, Coskun Kocabas and Atilla Aydinli

Department of Physics, Bilkent University, 06800, Ankara, Turkey

E-mail: aydinli@fen.bilkent.edu.tr

Received 22 July 2003
Published 17 December 2003
Online at stacks.iop.org/JMM/14/374 (DOI: 10.1088/0960-1317/14/3/009)

Abstract
We describe a novel displacement sensor for scanning probe microscopies using an integrated optical micro ring resonator. This device operates by means of monitoring the changes in the transmission spectrum of a high finesse micro ring resonator. Finite element method simulations were carried out to obtain the optimum sensor design and finite difference time domain simulation was used to obtain the transfer characteristics of micro ring resonators. Operation principles and sensitivity calculations are discussed in detail. To achieve high sensitivity, we have studied different types of ring resonator. The highest sensitivity is obtained in a race-track resonator. This new design should provide sensitivities as high as $\sim 10^{-4}$ Å^{-1}.

1. Introduction

Many scanning probe microscopies require the measurement of displacement with high sensitivity. A good example is atomic force microscopy (AFM) [1], based upon the principle of sensing the forces between a tip and a surface. These forces induce the displacement of the tip mounted on a cantilever. There is a great need to determine the displacement of the cantilever with high sensitivity, to work out the attractive and repulsive forces between the surface and the tip. There are many methods to determine the tip displacement: tunnelling [1], optical lever [2], interferometry [3], piezoresistive [4] and piezoelectric detections [5] and interdigital detection [6] techniques.

In this paper, we introduce integrated optical detection. This method has many advantages over others. First, an integrated sensor does not require any alignment while scanning the surface and it is possible to scan large areas. Secondly, integrated sensors are suitable for cantilever arrays due to their compactness, simplicity and potential for mass production. It should also be mentioned that integrated sensors such as piezoresistive sensors [4] have less sensitivity than external sensors such as optical levers [2]. Using an integrated optical sensor, we expect to achieve a sensitivity as high as that of external sensors. Integrated optical devices can be inexpensive and they can be used in harsh environments such as ultra-high vacuum (UHV) systems and electromagnetically active environments. Recently there have been several studies on integrated optic pressure sensors, biosensors, temperature sensors and strain sensors. These sensors consist of an integrated optical device, such as a Mach–Zehnder interferometer [7], a directional coupler [8] and a ring resonator [9], whose transmission characteristics change due to external effects.

In this paper, we propose for the first time a new integrated optical sensor for scanning probe microscopes. In this design, an optical waveguide coupled to a high finesse micro ring resonator integrated with a cantilever is used as a strain sensor to deduce displacement. Basically, stress due to displacement of the cantilever changes the local refractive index on the ring resonator through the photo-elastic effect and index change causes modifications in the transmission characteristics of the optical waveguide coupled ring resonator. Monitoring the intensity modulation through the optical waveguide, it is possible to determine the cantilever displacement with high accuracy. Finite element method (FEM) simulations were carried out to obtain the optimum sensor design and finite difference time domain (FDTD) simulations were used to obtain the transmission characteristics of optical waveguide coupled ring resonators. To achieve high sensitivity, we have studied different types of ring resonator. The highest sensitivity was obtained for race-track resonators.

0960-1317/04/030374+08$30.00 © 2004 IOP Publishing Ltd Printed in the UK

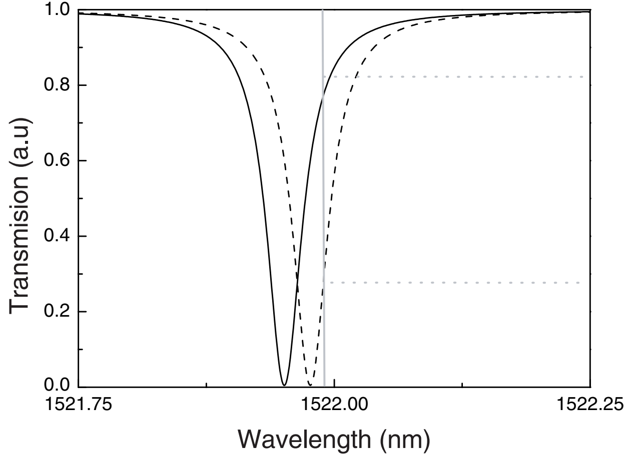

Figure 1. Sensor concept based on a ring resonator. The optical power modulation takes place as the position of resonance dip shifts due to the displacement of the cantilever.

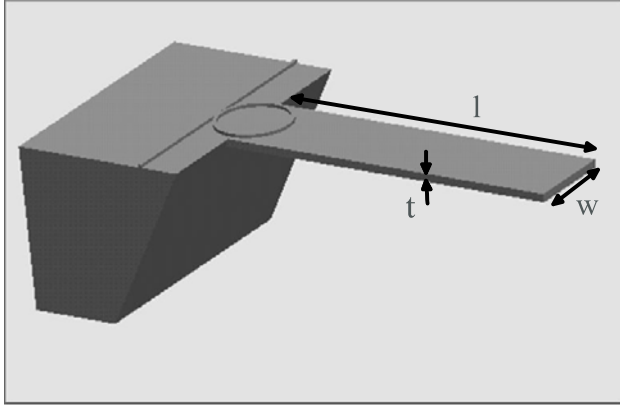

Figure 2. Schematic diagram of the cantilever integrated with the micro ring resonator. l, t and w represent the length, thickness and width of the cantilever, respectively.

2. Physical considerations

In the method employed in this work [10], a micro ring resonator integrated on a cantilever is used to measure displacement. (A detailed analysis of micro ring resonators is discussed in the next section.) The atomic forces make the cantilever deflect from equilibrium and this deflection produces stress on the cantilever surface. The index change on the ring due to the stress causes a shift in the resonant wavelength. Figure 1 shows the transmission spectrum of an optical waveguide coupled to a ring resonator, and the modulation concept. The stress reaches its maximum value at the supporting point of the cantilever and it decreases linearly along the cantilever. Maximum stress on the surface of the base of the cantilever as a function of tip displacement, z, can be written as

$$\sigma_{\max} = \frac{3Et}{2l^2} z \tag{1}$$

where E is the Young's modulus of the cantilever material, t is the thickness, and l is the length of the cantilever (see figure 2). Due to the photo-elastic effect, the effective index

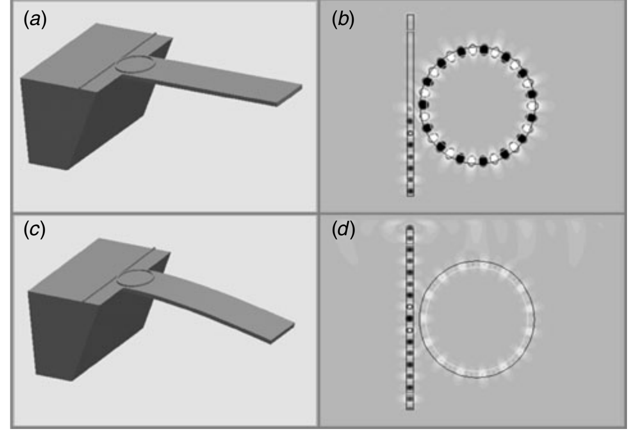

Figure 3. A schematic illustration of the operational principle for the integrated micro ring resonator displacement sensor: (a), (c) the cantilever for unbent and bent conditions; (b), (d) the field distribution on the ring resonator on the cantilever.

changes due to the stress and through the equation

$$n_{\text{eff}} = n_0 + \sum_i C_i \sigma_i \tag{2}$$

where C_i is the stress optic constant of waveguide and σ_i is the local stress. For GaAs longitudinal and transverse stress optic coefficients are 1.7×10^{-11} Pa^{-1} and 1×10^{-11} Pa^{-1}, respectively [11]. Longitudinal stress is much larger than the transverse stress, which can be neglected, so that

$$\Delta n_{\max} \simeq C_l \sigma_l \simeq \frac{3C_l E t}{2l^2} z. \tag{3}$$

The change in refractive index can also be written as a function of the force applied to the tip. From Hooke's law, the force on the rectangular cantilever can be expressed as

$$F = kz = \frac{wEt^3}{4l^3} z \tag{4}$$

where k denotes the spring constant of the cantilever. Then the change in refractive index can be written as

$$\Delta n_{\max} \simeq \frac{6C_l l}{wt^2} F. \tag{5}$$

From equations (4) and (5), the refractive index change depends on the geometry of cantilever and the photo-elastic constant of the material. As the stress-induced index change is not uniform on the ring, the total accumulated round trip phase on the ring can be written as

$$\Delta\Phi = \frac{2\pi}{\lambda} \int_{\text{ring}} \Delta n \, \text{d}l \simeq \frac{2\pi C_l}{\lambda} \int_{\text{ring}} \sigma_l \, \text{d}l \tag{6}$$

where λ is the wavelength. In order to achieve large phase shifts, the total length of the ring must be kept large and a cantilever material with a large elasto-optic coefficient must be chosen. Figure 3 shows a schematic illustration of the operational principle for the integrated micro ring resonator displacement sensor, extracted from a FDTD simulation.

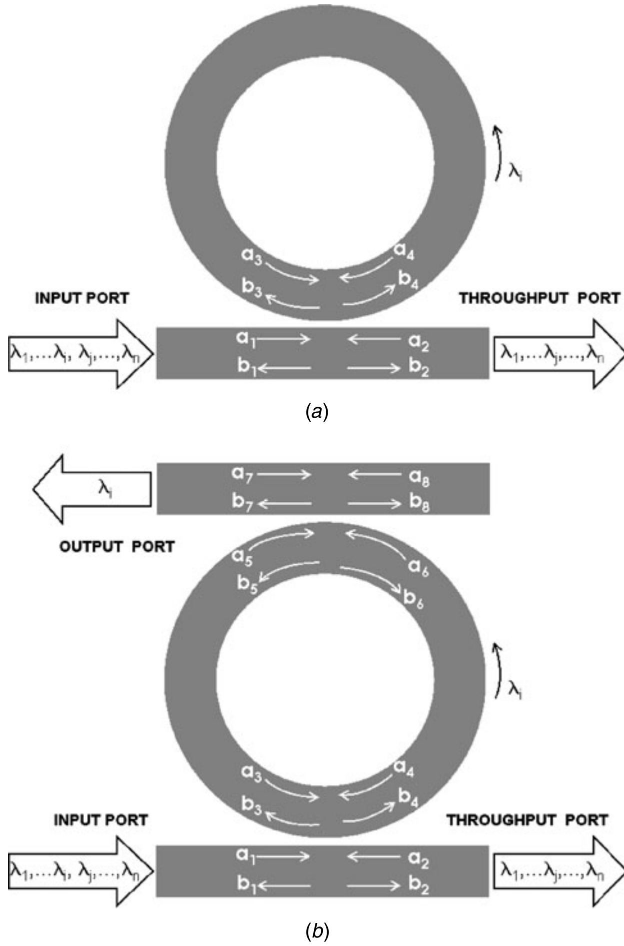

Figure 4. Schematic representation of single-bus (*a*) and double-bus (*b*) ring resonators and the relevant propagating field amplitudes.

3. Analysis and design of micro ring resonators

Micro ring resonators are of great interest due to their compactness, the fact that they do not need facets or gratings for optical feedback, their stability with respect to back reflections and high wavelength selectivity, which are key features for various applications. They mainly find applications in wavelength division multiplexing (WDM) [12] and wavelength add-drop systems [13] for optical communications. Ring resonators are not only good candidates for WDM and add/drop filters but also well suited for routing [14], switching and modulation applications [15].

3.1. Ring resonator analysis: single bus system

A ring resonator system may be composed of one or two bus waveguides and a ring placed very close to them as shown in figure 4. There are several figures of merit for a ring resonator. These are the modulation depth which shows the depth of the on/off ratio (in dB), free spectral range (FSR) which is the wavelength spacing between adjacent resonances, full width at half-maximum (FWHM) which is resonance peak width at half-maximum power. The Q factor gives the ratio of resonance wavelength to FWHM of the resonance. Depending on the application, large or small values for FSR may be desirable but small FWHMs, large modulation depths and large Q factors are always preferred.

Consider the single bus coupled ring structure in figure 4(*a*). The general matrix for outgoing waves in terms of incoming waves in the coupling region of the system [16] is

$$\begin{bmatrix} b1 \\ b2 \\ b3 \\ b4 \end{bmatrix} = \begin{bmatrix} 0 & (1-k^2)^{1/2} & 0 & \mathrm{i}k \\ (1-k^2)^{1/2} & 0 & \mathrm{i}k & 0 \\ 0 & \mathrm{i}k & 0 & (1-k^2)^{1/2} \\ \mathrm{i}k & 0 & (1-k^2)^{1/2} & 0 \end{bmatrix} \begin{bmatrix} a1 \\ a2 \\ a3 \\ a4 \end{bmatrix}. \quad (7)$$

Here, $|k|^2$ is the fraction of power coupled between waveguide and ring, so that $1-|k|^2$ is the transmitted portion of the power that is not coupled to the ring. In the case of no back reflections and a_1 being the input wave

$$a_2 = a_4 = b_1 = b_3 = 0. \quad (8)$$

Then, solving the matrix for the remaining terms leads to transmitted amplitudes as

$$b_2 = (1-k^2)^{1/2} a_1 + \mathrm{i}k a_3 \quad (9)$$

and

$$b_4 = (1-k^2)^{1/2} a_3 + \mathrm{i}k a_1. \quad (10)$$

Matching the travelling waves in the ring gives

$$a_3 = b_4 \exp(-(\alpha_T + \mathrm{i}\phi)) \quad (11)$$

and using this to eliminate a_3 in the above equations results in

$$b_2 = \frac{(1-k^2)^{1/2} - \exp(-(\alpha_T + \mathrm{i}\phi))}{1-(1-k^2)^{1/2}\exp(-(\alpha_T + \mathrm{i}\phi))} a_1 \quad (12)$$

where α_T and ϕ are the optical loss and phase accumulated per round trip in the ring, respectively. For a resonator of length L ($=2\pi R$), optical loss coefficient α and effective refractive index of n_e

$$\alpha_T = \alpha L \quad (13)$$

and

$$\phi(\lambda) = \frac{2\pi}{\lambda} n_e L \quad (14)$$

where λ is the free space wavelength. The resonance takes place when $\phi = 2\pi m$, and m is an integer number. Then, the resonance field amplitudes become

$$b_2 = \frac{(1-k^2)^{1/2} - \exp(-\alpha_T)}{1-(1-k^2)^{1/2}\exp(-\alpha_T)} a_1 \quad (15)$$

and

$$b_4 = \frac{\mathrm{i}k}{1-(1-k^2)^{1/2}\exp(-\alpha_T)} a_1. \quad (16)$$

An obvious result is that if

$$(1-k^2)^{1/2} = \exp(-\alpha_T) \quad (17)$$

no power is reflected so that $b_2 = 0$. This is the so-called critical coupling condition and all the power is coupled to the ring. It is necessary to take the square of the field b_2 and b_4 to find the corresponding optical intensities in terms of the input optical power. Therefore, the transmitted power at

resonance is

$$I_t = |b_2|^2 = \left| \frac{(1-k^2)^{1/2} - \exp(-(\alpha_T + \mathrm{i}\phi))}{1-(1-k^2)^{1/2}\exp(-(\alpha_T + \mathrm{i}\phi))} a_1 \right|^2. \quad (18)$$

3.2. Ring resonator analysis: double bus system

The above treatment can be easily extended to a ring structure coupled to two buses as shown in figure 4(*b*). When there is a second bus, there will be a second coupling region allowing for the out coupling of trapped light in the ring. The expression for reflected power is exactly the same as in the single bus system apart from a change in the loss term to account for the coupled power to the second bus. The new loss term is

$$\alpha_{\mathrm{eff}} = -\ln\left(1-k_2^2\right)^{1/2} + \alpha_T. \quad (19)$$

So, the new transmitted intensity is

$$I_t = \left| \frac{(1-k^2)^{1/2} - \exp(-(\alpha_{\mathrm{eff}} + \mathrm{i}\phi))}{1-(1-k^2)^{1/2}\exp(-(\alpha_{\mathrm{eff}} + \mathrm{i}\phi))} a_1 \right|^2 \quad (20)$$

Here, $|k_1|^2$ is $|k|^2$ and $|k_2|^2$ is the fraction of power coupled between the second bus and the ring. In most cases $|k_1|^2 = |k_2|^2 = |k|^2$. Analysing the resonances and imposing that no reflected power takes place, i.e. $I_t = 0$, gives the critical coupling condition for the double bus system at resonance as

$$\left(1-k_1^2\right)^{1/2} = \left(1-k_2^2\right)^{1/2}\exp(-\alpha_T). \quad (21)$$

3.3. Waveguide design

We design and analyse ring resonators on a GaAs/AlGaAs platform. The waveguides designed are deeply etched to achieve strong confinement [17], which is essential to minimize waveguide bending losses. The general waveguide structure is seen in figure 5(*a*). The fraction of Al, *x*, and the geometry of the waveguide are chosen so that single mode propagation is ensured. The basic limitation to the resonator, and therefore to the waveguide design, is the need to propagate light in a small radius of curvature of less than 25 μm with minimum loss, since a typical cantilever width is about 50 μm. In principle, we need to find the complex angular propagation constant, γ, for a bend of radius R, using

$$n_{\mathrm{bend}} = \frac{\mathrm{Re}(\gamma)}{k_0 R} \quad (22)$$

to find the effective refractive index of the bend [18]. The condition for guiding light in a bending waveguide is that n_{bend} should be larger than substrate refractive index, n_{sub}. Determining n_{bend} requires solving the wave equation in cylindrical coordinates or employing full numerical calculations of the propagation constant by the beam propagation method (BPM) or the FDTD method, both of which are tedious. As a first-order approximation, we use an empirical equation [19] for the cut-off radius, R_{co}, in terms of waveguide width, w, refractive indices of straight waveguide, n_{str}, and substrate, n_{sub}, which is

$$R_{\mathrm{co}} = \frac{w n_{\mathrm{rib}}}{2(n_{\mathrm{str}} - n_{\mathrm{sub}})}. \quad (23)$$

A few trials with different Al mole fraction, waveguide width, w, and height, H, led us to a single mode waveguide structure which can be fabricated using optical lithography.

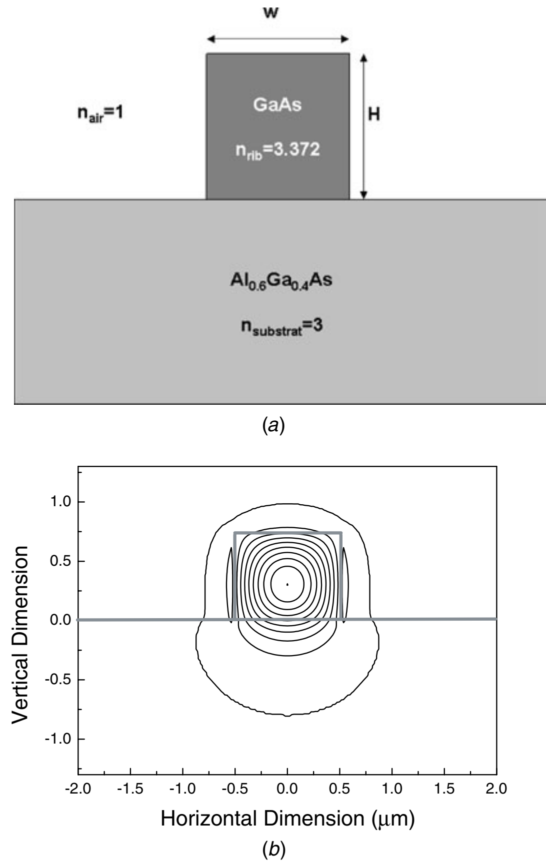

Figure 5. Single-mode waveguide structure (*a*), and its mode distribution (*b*).

This structure has 0.6 as x, 1 and 0.75 μm as w and H respectively. n_{str} is 3.192 for TE polarization which is found by mode calculation using a commercial BPM program (see figure 5(*b*)), $n_{\mathrm{rib}} = n_{\mathrm{GaAs}}$ is 3.372 and $n_{\mathrm{subst}} = n_{\mathrm{AlGaAs}}$ is 3.000. This structure gives a value of R_{co} of 9 μm. We have chosen this to be safe to use an R value of 20 μm for the ring.

3.4. Ring resonator as displacement sensor

For the purpose of sensing displacement, we are mainly interested in modulation applications of ring resonators. It should be possible to obtain a large modulation in transmitted optical power by small variations of the refractive index. This type of modulation is useful only if the resonance wavelength shift remains in the bandwidth of the resonator. Such shifts can only be achieved through a controllable change in optical path length of resonators, which is a function of resonator physical length and effective refractive index. Here, stress-induced refractive index change is employed. When the ring resonator is designed to have a high Q factor, the modulation is dramatic due to steep fall of the transmission dip. A ring resonator could have high Q factors when designed to work at the critical coupling regime.

As the operational principle of the ring resonator coupled waveguide sensor depends on the stress distribution along the cantilever, we have calculated the three-dimensional (3D) stress distribution using FEM simulations, for which we used a Young's modulus of 0.86×10^{11} N m^{-2} and a Poisson ratio

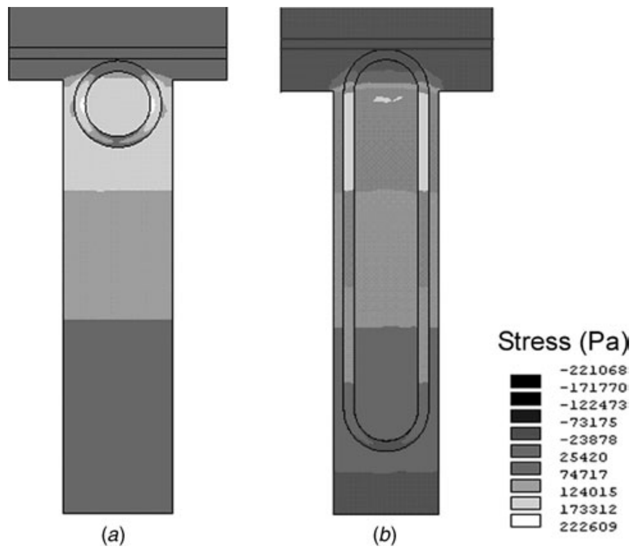

Figure 6. Longitudinal stress distribution on the cantilevers with ring (*a*) and race-track (*b*) shape resonators. Long straight arms in the race-track resonators are useful for increasing the accumulated phase shift.

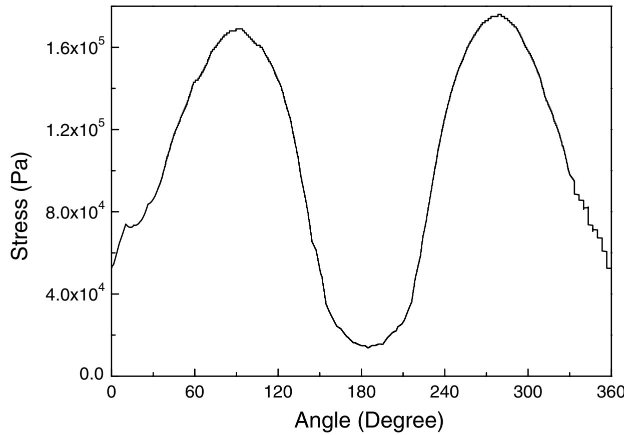

Figure 7. Calculated stress distribution on the surface of the ring resonator for 100 A tip displacement as a function of the angle between the major symmetry axes of the cantilever.

of 0.31. Static stress analysis was performed using ANSYS software. The mesh was increased in the region where the ring resonator was placed. The analysis performed here uses the stress at the surface. The local stress on the top surface decreases along the z-direction and becomes negative on the opposite surface. Figure 6(*a*) shows the stress contours on the the ring resonator obtained from the FEM simulation. Maximum stress occurs at the supporting point of the cantilever and decreases linearly along the cantilever. In figure 7, we plot the stress distribution along the circumference of the ring. From figure 7, it is clearly observed that large stress occurs on the two sides of the ring which are parallel with the major symmetry axis of the cantilever. The calculated total accumulated phase on the ring with a radius of 20 μm is 5×10^{-4} rad for 100 Å deflection of the cantilever. In order to increase the accumulated phase shift, the parallel sides may be kept longer. The optimum design is a race-track shaped resonator, because of its two long parallel sides where stress is much larger than the curved sides. Figure 6(*b*) shows the stress contours on the race-track resonator. Stress distribution reaches its maximum value on the surface of the waveguide and decreases linearly along its thickness. For the sensitivity calculations, we averaged stress along the thickness of the waveguide. The average value of the stress is equal to the stress in the middle of the waveguide where the intensity of the guided light is maximum. As the stress distribution is calculated with the waveguides on the surface of the cantilever, stress also varies along the width of the waveguides in the curved sections of the devices. We neglected the variation of stress in the curved sections and used the value of the stress in the middle of the waveguide in the calculations. The phase shift can be approximated as

$$\Delta\Phi \simeq \frac{3\pi C_l E t L_{\mathrm{rt}}}{2\lambda l^2} z \qquad (24)$$

where L_{rt} is the length of the race-track resonator. From equation (24), it is observed that the phase shift is linearly proportional to the cantilever deflection and it is related to the cantilever geometry and mechanical properties of the cantilever material. For higher sensitivity, the total length of the ring and the elasto-optic coefficient of the material must be large. The phase shift can also be written as a function of force applied to the tip so that

$$\Delta\Phi \simeq \frac{6\pi C_l l L_{\mathrm{rt}}}{\lambda w t^2} F \qquad (25)$$

where F is the applied force and w is the width of the cantilever. In order to increase the phase shift due to the applied force we have to keep the length long and the thickness of the cantilever small, which results in a trade-off between force and displacement sensitivity. It is not possible to achieve high displacement sensitivity as well as high force sensitivity. We can conclude that a short and thick cantilever is sensitive to displacement measurements whereas a long and thin cantilever is more sensitive for force detection. One interesting result which is seen from equation (25) is that the phase shift does not depend on the Young's modulus of the cantilever. For small displacements, output intensity is a linear function of displacement.

4. Cantilever design

The fundamental mechanical parameters of an AFM cantilever are its spring constant and resonant frequency. The optimal values of these parameters depend on the mode of the operations, namely contact mode, non-contact mode and intermittent contact mode. GaAs has a large photo-elastic constant which makes it a suitable material for fabrication of integrated optical devices and cantilevers [20–22]. Other materials such as Si_3N_4 and Si can also be used with varying sensitivities. Our design is based on rectangular cantilevers which are compatible with well-established micromechanical fabrication technology. Typical micromachined cantilevers for AFM have lengths of 100–400 μm, widths of 20–50 μm and thicknesses of 0.4–10 μm. A large spring constant is preferable for non-contact mode and intermittent mode operations. On the other hand, low force constant is preferable for contact mode operations. The resonant frequency is required to be a few kHz in order to minimize the external effects [23].

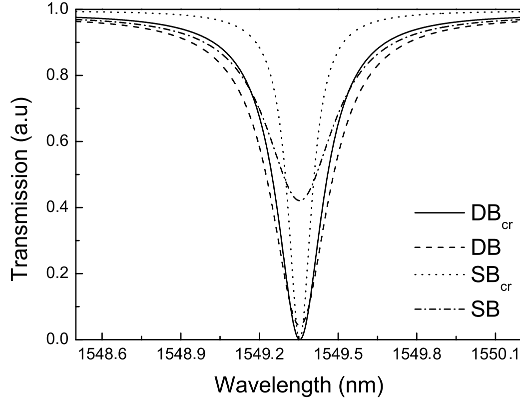

Figure 8. Transmission spectrum of single-bus and double-bus race-track resonators, both with (SB_{cr} and DB_{cr}) and without (SB and DB) the critical coupling condition, respectively. The increase in the slope of the resonance when critical coupling is achieved is clearly observed.

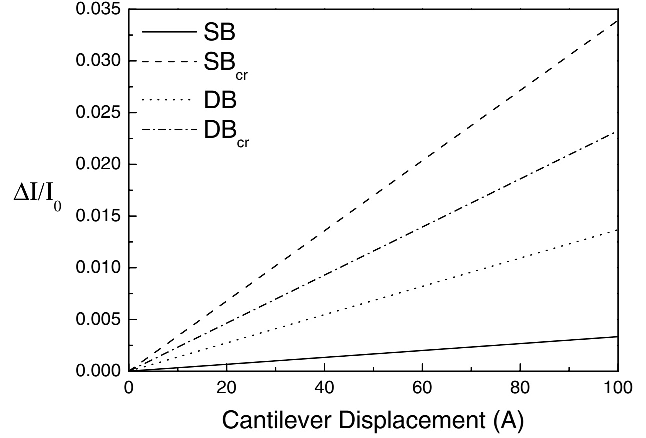

Figure 9. Transmitted intensity variation with cantilever displacement for single-bus and double-bus race-track resonators with (SB_{cr}, DB_{cr}) and without (SB, DB) the critical coupling condition achieved. The best results are obtained under critical coupling condition.

5. Sensitivity analysis

The sensitivity of displacement sensors is the essential property of the atomic force microscopies. The minimum detectable force and the displacement depend on the sensitivity of the sensor and the noise of the system. Integrated sensors have less sensitivity than external ones. There have been several studies to increase the sensitivity of the integrated sensor, but the best sensitivity achieved so far is $\sim 10^{-6}$ A^{-1} [20], which is two orders of magnitude less than the sensitivity of the interferometric detection [3]. Force sensitivity can be defined as the variation of the current on the detector per unit force applied to the tip. And with the same logic, displacement sensitivity can be defined as the variation of the current on the detector per unit displacement of the cantilever. The current on the detector is proportional to the light falling on it

$$i = \frac{\eta I_t}{h\nu} \tag{26}$$

where η is the quantum efficiency of the photodetector, I_0 is the incident optical power and ν is the frequency of the light. Therefore

$$\frac{\Delta i}{i_0} = \frac{\Delta I}{I_0}. \tag{27}$$

The detected power, I_t, depends on the transmission characteristics of the ring resonator coupled waveguide. Transmissions of the single and double bus ring resonators are given in equations (18) and (20), respectively. In figure 8, we plot the transmission spectrum for single bus and double bus resonators with and without the critical coupling condition. Achieving the critical coupling condition, it is possible to have very high modulation depth and very narrow spectral response. Output intensity variation with cantilever displacement is given in figure 9. We can write displacement and force sensitivities as

$$S_d = \frac{\Delta I_t}{I_0 \Delta z} = \frac{1}{I_0}\frac{\mathrm{d}I_t}{\mathrm{d}\phi}\frac{\mathrm{d}\phi}{\mathrm{d}z} \tag{28}$$

and

$$S_f = \frac{\Delta I_t}{I_0 \Delta F} = \frac{1}{I_0}\frac{\mathrm{d}I_t}{\mathrm{d}\phi}\frac{\mathrm{d}\phi}{\mathrm{d}F}. \tag{29}$$

Table 1. Calculated displacement sensitivities for single and double bus ring resonator with (SB_{cr}, DB_{cr}) and without (SB, DB) critical coupling condition achieved.

Device	SB	SB_{cr}	DB	DB_{cr}
Sensitivity (Å^{-1})	3.37×10^{-5}	3.39×10^{-4}	1.37×10^{-4}	2.33×10^{-4}

In table 1, we compare the calculated sensitivities of the ring resonators for single bus and double bus configurations with and without the critical coupling condition. The highest sensitivities are achieved under critical coupling conditions. The sensitivity of the ring resonator is wavelength-dependent. Figure 10 shows the wavelength dependence of the race-track ring resonator. The most sensitive operation can be achieved at the wavelength for which the output intensity has the steepest slope. The calculated sensitivities are promising and it should be possible to achieve sensitivities as high as the sensitivity of the interferometric detection. The sensitivity of the detector depends mainly on the design of the resonator and the waveguide. Considering the round trip losses, we design the resonator to accomplish the critical coupling condition. To achieve critical coupling, the gap between the straight waveguide and the ring should be precisely controlled. In our design we estimate propagation loss to be of the order of 10 dB cm^{-1} for waveguides. Under this condition, the gap size for critical coupling should be lower than $0.1\ \mu$m, which can be defined by e-beam but not by optical lithography. The solution for optical lithographic fabrication would be to vertically couple the ring resonator and the bus waveguide [24], for which the coupling gap can be controlled precisely through standard deposition or epitaxial growth techniques. However, even if critical coupling is not achieved, the calculated sensitivities are still very good, especially for the double bus structure. In the double bus structure, the second bus can be placed next to the ring but opposite to the first waveguide.

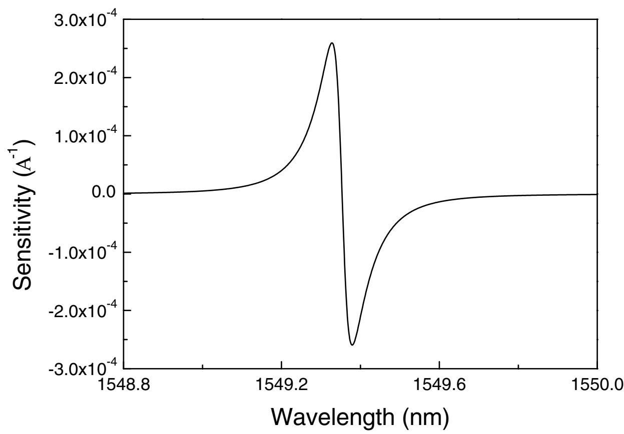

Figure 10. Sensitivity versus wavelength for the single-bus race-track resonator with critical coupling achieved.

6. Noise considerations

The resolution of a scanning force microscope is limited by the noise of the system. The minimum detectable distance (MDD) depends not only on the sensitivity but also on the noise of the microscope. The noise level of the system establishes the minimum detectable optical power on the photodetector necessary to obtain the cantilever displacement. For piezoresistive cantilevers, the fundamental noise is the Johnson noise in the piezoresistor [25]. For optical lever [2] and interdigital detection techniques, the fundamental noises are the shot noise of the photodetector and thermal vibration of the cantilever [6].

Displacement sensitivity is defined as the variation of the normalized output intensity per unit displacement of the tip. It can be written as

$$S = \frac{\Delta I}{I_0 \Delta z}. \qquad (30)$$

The input intensity (power), I_0, depends on the light source and typically is of the order of few mW. There are several noise sources in a displacement measuring cantilever system using integrated optical detection. The laser used to provide the signal is a source of noise. Not only the output intensity but also the phase and the frequency of a semiconductor laser fluctuate in time. The cantilever displacement is measured directly from the optical intensity changes in the transmission spectrum of the ring resonator system, therefore magnitudes of these fluctuations should be estimated. For a semiconductor laser, the intensity fluctuation noise is given as the relative intensity noise (RIN)

$$\mathrm{RIN} = \frac{(\delta P)^2}{P^2} \qquad (31)$$

and DFB lasers with RIN of 160 dB Hz^{-1} are commercially available. This noise exists for both ring and race-track resonators used to detect cantilever displacement in this work. The laser intensity variation can be eliminated by introducing a reference photodetector and using differential amplification, and the output intensity can be normalized. For this design a tunable laser source is chosen which provides high intensity and wavelength stability [27]. This laser provides 0.01 dB long-term intensity stability which translates into power variation of 0.1%. Another important noise source is the random wavelength variations. For ring and race-track resonator displacement sensors, the wavelength variation causes output intensity variation. In order to reduce this noise, a laser which provides high wavelength stability can be used. There are commercially available tunable lasers with 0.1 pm wavelength stability which introduce intensity variation of 0.01% [27]. The intensity variation and wavelength variation can be reduced by using suitable light sources and lock-in amplification. On the other hand, laser pointing noise that needs to be considered for external optical detection methods is eliminated in this work. Since the laser is butt-coupled to the waveguide, this eliminates pointing noise. An additional noise source is due to the thermal vibration of the cantilever. To analyse the thermal vibrational noise, the cantilever can be modelled as a simple harmonic oscillator. At finite temperatures, the cantilever vibrates due to thermal excitation. The thermal mechanical noise of the cantilever is estimated as [28]

$$\Delta z_{\mathrm{thermal}} = \sqrt{\frac{2k_b T B}{\pi Q k f_0}} \qquad (32)$$

where k_b is the Boltzmann constant, T is the temperature, B is the bandwidth, Q is the quality factor of the cantilever, k is the spring constant and f_0 is the resonance frequency of the cantilever. To estimate the magnitude of the noise, a rectangular cantilever with length of 200 μm, width of 50 μm and thickness of 5 μm is chosen. The resonance frequency is 50 kHz, the spring constant is 16 N m^{-1} and the bandwidth is about 1 kHz. The quality factor of the cantilever $Q = 100$ is chosen for this analysis. At room temperature, the thermal vibrational noise is obtained as $\Delta z_{\mathrm{thermal}} = 0.0017$ Å which is very small.

Finally, there are two fundamental noises for detection electronics: shot noise and thermal noise. These noises are fundamental noises and cannot be eliminated. Shot noise is a fundamental noise that exists in all optical detection processes. When the optical power is detected, photons fall randomly on the photodetector and the time average of the received power fluctuates due to this randomness. The rms current due to shot noise is given by the well-known equation as

$$i_{\mathrm{shot}} = \sqrt{2e\mathrm{i}B} \qquad (33)$$

where e is the electron charge and B is the bandwidth. The signal-to-noise ratio (SNR) can be written as

$$\mathrm{SNR} = \frac{\mathrm{i}}{i_{\mathrm{shot}}} = \sqrt{\frac{\mathrm{i}}{2eB}}. \qquad (34)$$

SNR increases with the received power. For 100 μW optical power the shot noise current is $i_{\mathrm{shot}} = 6 \times 10^{-10}$ A, SNR is 10^5 and shot noise limited MDD is 0.027 Å. Another noise source for photodetectors is the thermal noise in the detection electronics, also known as Johnson noise. Random thermal motion of the electrons in a resistor produces a fluctuating current given by

$$i_{\mathrm{thermal}} = \sqrt{\frac{4kTB}{R}} \qquad (35)$$

where k is the Boltzmann constant, T is the temperature and R is the resistance. A typical value of thermal noise

is $i_{\text{thermal}} = 4 \times 10^{-10}$ A. The total noise is the sum of all the noise contributions. If the received power is high enough, the dominant noise becomes the shot noise and determines the noise level of the system. Generally, for all scanning force microscopes which use optical detection the dominant noise source is the shot noise. For $100\,\mu$W optical power, shot noise limited MDD is 0.027 Å. The SNR can be increased by increasing the optical power.

7. Conclusions

In this paper, we propose a novel integrated ring resonator displacement sensor for scanning probe microscopies. We design and analyse the feasibility of the integrated optical sensor. We discuss the concept based on the elasto-optic effect. We have described the design of the ring resonator and presented a theoretical investigation of the force and displacement sensitivity. The design of GaAs-based cantilever with integrated ring and race-track resonators has been described in detail. We find that the integrated optical sensor is attractive because of its high sensitivity and simplicity. We introduce a new application area for integrated optics. This design is a good alternative for piezoresistive cantilevers especially in electromagnetically active environments. Integrated sensors are suitable for cantilever arrays due to their compactness, simplicity and compatibility with mass production. The main advantages of this method are that it does not need any alignment, it is a compact set-up and it has high sensitivity.

Acknowledgments

We would like to thank Professor A Oral for an introductory discussion on cantilever design. This work was supported by Bilkent University Research Fund (Phys-03-02) and the Scientific and Technical Research Council of Turkey (TUBITAK Project No 199E006).

References

[1] Binning G, Quate C and Gerber Ch 1986 Atomic force microscope *Phys. Rev. Lett.* **56** 930–3

[2] Meyer G and Amer N M 1988 Novel optical approach to atomic force microscopy *Appl. Phys. Lett.* **53** 1045–7

[3] Rugar D, Mamin H J and Guethner P 1989 Improved fiber-optic interferometer for atomic force microscopy *Appl. Phys. Lett.* **55** 2588–90

[4] Tortonese M, Yamada H, Barrett R C and Quate C F 1991 Atomic force microscopy using a piezoresistive cantilever 1991 *Proc. IEEE Conf. on Tranducers (1991)* 448–51

[5] Akamine S, Albrecht T R, Zdeblick M J and Quate C F 1989 Microfabricated scanning tunneling microscope *IEEE Electron Device Lett.* **10** 490–92

[6] Manalis S R, Minne S C, Atalar A and Quate C F 1996 Interdigital cantilever for atomic force microscopy *Appl. Phys. Lett.* **69** 3944–6

[7] Wagner C, Frankenberger J and Daimel P P 1993 Optical pressure sensor based on Mach–Zehnder interferometer integrated with a lateral a-Si:H p–i–n photodiode *IEEE Electron Device Lett.* **10** 1257–9

[8] Luff B J, Harris R D, Wilkinson J S, Wilson R and Schiffirin D J 1996 Integrated-optical directional coupler biosensor *Opt. Lett.* **21** 618–20

[9] De Brabander G N, Boyd J T and Beheim G 1994 Integrated optical ring resonator with micromechanical diaphragm for pressure sensing *IEEE Photon. Technol. Lett.* **6** 671–3

[10] Aydinli A and Kocabas C PCT application with application no PCT/TR03/053 (filed on 18 June 2003) Integrated Optical Sensors for Scaning Probe Microscopies

[11] Okamoto K 2000 *Fundamentals of Optical Waveguide* (New York: Academic) p 265

[12] Kohtoku M, Oku S, Kadota Y, Shibata Y and Yoshikuni Y 2000 200-GHz FSR periodic multi-demultiplexer with flattened transmission and rejection band by using a Mach–Zehnder interferometer with a ring resonator *IEEE Photon. Technol. Lett.* **12** 1174–6

[13] Little B E, Foresi J S, Steinmeyer G, Thoen E R, Chu S T, Haus H A, Ippen E P, Kimerling L C and Greene W 1998 Ultra-compact Si-SiO_2 microring resonator optical channel dropping filters *IEEE Photon. Technol. Lett.* **10** 549–51

[14] Little B E, Haus H A, Foresi J S, Kimerling L C, Ippen E P and Ripin D J 1998 Wavelength switching and routing using absorption and resonance *IEEE Photon. Technol. Lett.* **10** 816–918

[15] Choi J M, Lee R K and Yariv A 2001 Control of critical coupling in a ring resonator-fiber configuration: application to wavelength-selective switching, modulation, amplification, and oscillation *Opt. Lett.* **26** 1236–8

[16] Altman J L 1964 *Microwave Circuits* (Princeton, NJ: Van-Nostrand)

[17] Chin M K and Ho S T 1998 Design and modeling of waveguide-coupled single-mode microring resonators *J. Lightwave Technol.* **16** 1433–46

[18] Kim S and Gopinath A 1998 Vector analysis of optical dielectric waveguide bends using finite-difference method *J. Lightwave Technol.* **14** 2085–92

[19] Pennings E C M, Deri R J and Hawkins R J 1991 Simple method for estimating usable bend radii of deeply etched optical rib waveguides *Electron. Lett.* **27** 1532–4

[20] Brook A J, Bending S J, Pinto J, Oral A, Ritchie D, Beere H, Springthorpe A and Henini M 2003 Micromachined III-V cantilevers for AFM-tracking scanning hall probe microscopy *J. Micromech. Microeng.* **13** 124–8

[21] Brook A J, Bending S J, Pinto J, Oral A, Ritchie D, Beere H, Henini M and Springthorpe A 2003 Integrated piezoresistive sensors for atomic force-guided scanning Hall probe microscopy *Appl. Phys. Lett.* **82** 3538–40

[22] Beck R G, Eriksson M A, Topinka M A, Westervelt R M, Maranowski K D and Gossard A C 1998 GaAs/AlGaAs self-sensing cantilevers for low temperature scanning probe microscopy *Appl. Phys. Lett.* **73** 1149–51

[23] Tortonese M 1997 Cantilevers and tips for atomic force microscopy *IEEE Eng. Med. Biol.* **16** 28–33

[24] Little B E, Chu S T, Pan W, Ripin D, Kaneko T, Kokubun Y and Ippen E 1993 Vertically coupled glass microring resonator channel droping filters *IEEE Photon. Technol. Lett.* **11** 215–7

[25] Hansen O and Boisen A 1999 Noise in piezoresistive atomic force microscopy *Nanotechnology* **10** 51–60

[26] ILX Lightwave Corp. *79800D DFB Source Module*

[27] ILX Lightwave Corp. *Tunable laser Source TLS 8800 Series*

[28] Rast S, Wattinger C, Gysin U and Meyer E 2000 The noise of cantilever *Nanotechnology* **11** 169–72